

# 1 **Unexpectedly high concentrations of atmospheric mercury** 2 **species in Lhasa, the largest city on the Tibetan Plateau**

3 Huiming Lin<sup>1</sup>, Yindong Tong<sup>2,3\*</sup>, Long Chen<sup>4</sup>, Chenghao Yu<sup>5</sup>, Zhaohan Chu<sup>1</sup>, Qianru  
4 Zhang<sup>1</sup>, Xiufeng Yin<sup>6</sup>, Qiangong Zhang<sup>7,8</sup>, Shichang Kang<sup>6,8</sup>, Junfeng Liu<sup>1</sup>, James  
5 Schauer<sup>9,10</sup>, Benjamin de Foy<sup>11</sup>, Xuejun Wang<sup>1\*\*</sup>

6 1. MOE Laboratory of Earth Surface Processes, College of Urban and Environmental Sciences, Peking  
7 University, Beijing 100871, China;

8 2. School of Science, Tibet University, Lhasa 850000, China

9 3. School of Environmental Science and Engineering, Tianjin University, Tianjin, 300072, China;

10 4. School of Geographic Sciences, East China Normal University, Shanghai 200241, China;

11 5. Key Laboratory of Microbial Technology for Industrial Pollution Control of Zhejiang Province,  
12 College of Environment, Zhejiang University of Technology, Hangzhou 310014, China

13 6. State Key Laboratory of Cryospheric Science, Northwest Institute of Eco-Environment and Resources,  
14 Chinese Academy of Sciences, Lanzhou 730000, China

15 7. Key Laboratory of Tibetan Environment Changes and Land Surface Processes, Institute of Tibetan  
16 Plateau Research, Chinese Academy of Sciences, Beijing, 100101, China;

17 8. CAS Center for Excellence in Tibetan Plateau Earth Sciences, Beijing, 100085, China;

18 9. Department of Civil and Environmental Engineering, University of Wisconsin-Madison, Madison, WI,  
19 USA;

20 10. Wisconsin State Laboratory of Hygiene, University of Wisconsin-Madison, WI, USA;

21 11. Department of Earth and Atmospheric Sciences, Saint Louis University, St. Louis, MO, 63108, USA

## 22 **Correspondence:**

23 \*Xuejun Wang (wangxuejun@pku.edu.cn) \*\*Yindong Tong (yindongtong@tju.edu.cn)

## 25 **Abstract**

26 Lhasa City is located in the central Tibetan Plateau and is the most densely populated area. As  
27 the first continuous monitoring of atmospheric mercury (Hg) species in a city on the Tibetan Plateau,  
28 our monitoring in Lhasa showed that the concentrations of gaseous elemental Hg (GEM), gaseous  
29 oxidized Hg (GOM), and particle-bound Hg (PBM) during subsequent of the Indian Summer  
30 Monsoon (S-ISM) period were  $2.73 \pm 1.48 \text{ ng m}^{-3}$ ,  $38.4 \pm 62.7 \text{ pg m}^{-3}$ , and  $59.1 \pm 181.0 \text{ pg m}^{-3}$ ,  
31 respectively. During the Westerly Circulation (WEC) period, the GEM, GOM and PBM  
32 concentrations were  $2.11 \pm 2.09 \text{ ng m}^{-3}$ ,  $35.8 \pm 43.3 \text{ pg m}^{-3}$ , and  $52.9 \pm 90.1 \text{ pg m}^{-3}$ , respectively.  
33 The GOM and PBM concentrations were higher than those of previous monitoring on the Tibetan  
34 Plateau and other provincial capitals in China. Typical high-value occurrence processes were studied  
35 to investigate random events with high atmospheric Hg concentrations in Lhasa. Combustion event

36 nearby or further away may be the main contributor of the high-concentration events. The lowest  
37 GEM concentrations occurred in the afternoon and persistently high concentrations were observed  
38 at night. The changes in GEM concentrations were consistent with the trends of other pollutant  
39 concentrations and contradictory to those of the wind speed. The high GEM concentrations at night  
40 can be attributed to the lower boundary layer height and lower wind speed. For both GOM and PBM,  
41 higher GOM concentrations occurred during the day and PBM during the night. The results of the  
42 principal component analysis indicated that local sources and wind speed are important factors  
43 influencing atmospheric Hg concentrations in Lhasa. The trajectory simulation showed that the  
44 source of the GEM in Lhasa gradually shifted from the south to the west of Lhasa from the S-ISM  
45 to the WEC periods, while both the southern and western sources were important in the late WEC  
46 period. The concentrations and change patterns of Hg species in Lhasa were significantly different  
47 than those at other monitoring sites on the Tibetan Plateau. Monitoring Hg species in Lhasa shows  
48 the possible maximum anthropogenic influences on the Tibetan Plateau and demonstrates the  
49 dramatic effect of wind on changes in urban atmospheric Hg concentrations.

50

## 51 **1. Introduction**

52 Mercury (Hg) has received worldwide attention owing to its high toxicity and bioaccumulation.  
53 Atmospheric mercury (Hg) exists in three different forms: atmospheric gaseous elemental Hg  
54 (GEM), gaseous oxidized Hg (GOM), and particle-bound Hg (PBM) (Selin, 2009). They exhibit  
55 different behaviors in the environment owing to their various chemical properties (Selin, 2009;  
56 Travnikov et al., 2017; Lindberg and Stratton, 1998; Seigneur et al., 2006). Many established  
57 monitoring networks for atmospheric Hg exist in North America and Europe (Stylo et al., 2016)  
58 including the Atmospheric Mercury Network (AMNet; Gay et al., 2013), the Global Mercury  
59 Observation System (GMOS; Sprovieri et al., 2013; Sprovieri et al., 2016), the Canadian  
60 Atmospheric Mercury Network (CAMNet; Kellerhals et al., 2003), and the Arctic Monitoring  
61 Assessment Programme (AMAP; <https://mercury.amap.no/>) (Gay et al., 2013; Sprovieri et al., 2013;  
62 Sprovieri et al., 2016; Kellerhals et al., 2003). They have been operating for decades and have  
63 provided a large amount of atmospheric Hg data. Compared to Europe and the United States,  
64 independent research teams have conducted monitoring work in China based on different research

65 interests (Fu et al., 2012a; Fu et al., 2008; Fu et al., 2016a; Fu et al., 2019; Fu et al., 2016b; Liu et  
66 al., 2011; Feng and Fu, 2016; Feng et al., 2013; Wang et al., 2015; Hu et al., 2014; Ci et al., 2011;  
67 Duan et al., 2017; Liu et al., 2002; Yin et al., 2018; Yin et al., 2020b; Lin et al., 2022; Lin et al.,  
68 2019). Most monitoring stations are set up only in developed regions, such as eastern and central  
69 China, owing to operational difficulties in remote areas. Few studies on atmospheric Hg in western  
70 China have been reported; thus, little is known about the overall level of atmospheric Hg in western  
71 China. To better employ the Minamata Convention and verify the effect of the implementation of  
72 the Convention, monitoring atmospheric Hg concentrations around the globe is significant and can  
73 aid in identifying the global Hg transport pattern.

74 The Tibetan Plateau is in the mid-latitudes of the Northern Hemisphere (in central Asia) and is  
75 an important area for studying the global Hg circulation. Owing to the high altitude and rough living  
76 conditions, there is little Hg research on the Tibetan Plateau. This area is less developed and there  
77 are few industrial activities; therefore, it is generally considered a clean region and can be treated  
78 as a background condition. However, there are large tourist cities in this area, such as Lhasa, where  
79 the number of tourists reached 40,121,522 in 2019 (Tibet Bureau of Statistics, 2020). Local cement  
80 production in Tibet reached 10.81 million tons in 2019 (Tibet Bureau of Statistics, 2020).  
81 Meanwhile, although the high altitude makes the Tibetan region a natural barrier between inland  
82 China and the Indian subcontinent (Qiu, 2008; Yao et al., 2012; Pant et al., 2018), the Tibetan Plateau  
83 is potentially influenced by the Indian summer monsoon (ISM) and the Westerly circulation (WEC).  
84 Trans-boundary inputs of atmospheric pollutants to the Tibetan Plateau have been demonstrated in  
85 pollutant studies such as with persistent organic pollutants and black carbon (Yang et al., 2018; Li  
86 et al., 2016b; Zhang et al., 2015b; Pokhrel et al., 2016; Wang et al., 2018; Zhang et al., 2015a; Feng  
87 et al., 2019; Zhu et al., 2019). Our previous study on atmospheric Hg in the Qomolangma region  
88 (QNNP) also suggested that atmospheric Hg from India can be transported and affect atmospheric  
89 Hg concentrations on the Tibetan Plateau as a result of the Indian monsoon (Lin et al., 2019). Hence,  
90 it remains unclear whether the Tibetan Plateau can be treated as a background area for studying  
91 atmospheric Hg, and further monitoring data are required. Monitoring in the largest cities on the  
92 Tibetan Plateau will provide important information and corroboration to address this query.

93 In previous study, Yin et al. (2018) reported GEM concentration data for the Namco region on

94 the Tibetan Plateau from 2012-2014 and found that the GEM concentration at Namco was  $1.33 \pm$   
95  $0.24 \text{ ng m}^{-3}$ , which is lower than the mean GEM concentration in the Northern Hemisphere  
96 (Lindberg et al., 2007; Slemr et al., 2015; Venter et al., 2015; Sprovieri et al., 2016; Lan et al., 2012).  
97 Our previous study at QNNP (Lin et al., 2019) showed that the atmospheric Hg concentrations were  
98  $1.42 \pm 0.37 \text{ ng m}^{-3}$ ,  $21.4 \pm 13.4 \text{ pg m}^{-3}$ , and  $25.6 \pm 19.1 \text{ pg m}^{-3}$  for GEM, GOM, and PBM,  
99 respectively, close similar to the average GEM concentrations in the Northern Hemisphere  
100 (Lindberg et al., 2007; Slemr et al., 2015; Venter et al., 2015; Sprovieri et al., 2016; Lan et al., 2012).  
101 The concentrations of atmospheric Hg species in Nyingchi, in the southeast Tibetan Plateau, were  
102 very low ( $1.01 \pm 0.27 \text{ ng m}^{-3}$ ,  $12.8 \pm 13.3 \text{ pg m}^{-3}$ , and  $9.3 \pm 5.9 \text{ pg m}^{-3}$  for GEM, GOM, and PBM,  
103 respectively), which may be affected by heavy wet deposition and the large amounts of vegetation  
104 in the Yarlung Zangbu/Brahmaputra Grand Canyon (Lin et al., 2022). However, Namco, QNNP  
105 and Nyingchi are remote areas on the Plateau, with few populations and industries. During previous  
106 studies in Lhasa, the largest city on the Plateau, only dry and wet depositions of atmospheric Hg  
107 were analyzed. Monitoring of atmospheric Hg particulate matter (Huang et al., 2016a) indicated that  
108 Lhasa has mean particulate Hg levels as high as  $224 \text{ pg m}^{-3}$  (ranging from  $61.2$  to  $831 \text{ pg m}^{-3}$ ),  
109 which is much higher than expected. Huang et al. (2013) measured the wet deposition of  
110 atmospheric Hg in Lhasa in 2010 and showed that the wet depositions of total Hg concentration and  
111 particulate Hg concentration were higher during the non-monsoon period than that during the  
112 monsoon period. The active Hg was higher during the monsoon than during the non-monsoon period,  
113 and they concluded that the wet deposition of Hg originated mainly from local sources. This  
114 indicates that atmospheric Hg concentrations in Lhasa may be elevated and further detailed  
115 monitoring is needed.

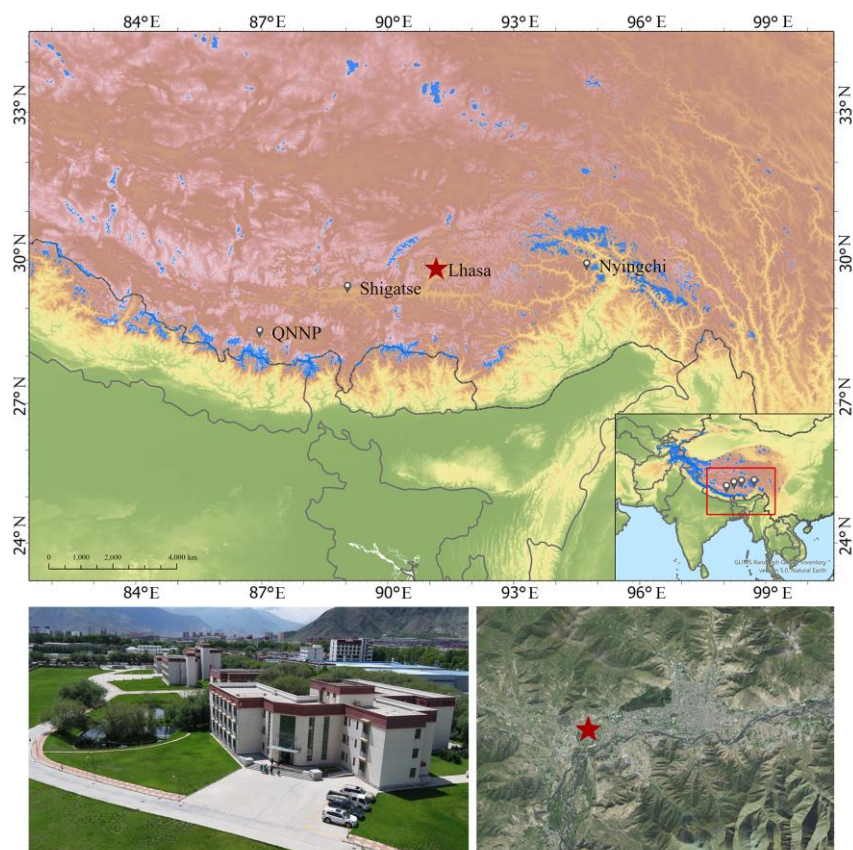
116 In this study, we conducted a high-time-precision atmospheric Hg species monitoring system  
117 in Lhasa. We performed continuous measurements of GEM, GOM, and PBM concentrations from  
118 subsequent of the Indian Summer Monsoon (S-ISM) period to the WEC period from 2016 to 2017.  
119 Based on literature research, this is the first continuous monitoring of atmospheric Hg species in a  
120 city on the Tibetan Plateau, and the influence of human activities, meteorological factors, and long-  
121 range transportation of pollutants on the diurnal variation of atmospheric Hg in Lhasa is discussed.  
122 We combined monitoring with other pollutant concentrations to explore the main factors influencing

123 the local atmospheric Hg concentrations. To determine the detailed source profile of atmospheric  
124 Hg, we combined real-time Hg monitoring data with backward trajectory and cluster analyses. This  
125 study can help understand atmospheric Hg characteristics in the city of the Plateau and provide  
126 scientific support for managerial decision-making.

## 127 **2. Material and methods**

### 128 **2.1 Atmospheric Hg monitoring sites**

129 The monitoring site for atmospheric Hg species in Lhasa was set up on the top floor of the  
130 Lhasa station office building in the Institute of Tibetan Plateau Research, Chinese Academy of  
131 Sciences, in western Lhasa City (29.64°N, 91.03°E, 3650 m above sea level; Figure 1, Figure S1).  
132 The monitoring in Lhasa included the subsequent Indian Summer Monsoon (S-ISM, August 29 to  
133 September 30, 2016) and Westerly Circulation (WEC, October 1, 2016 to February 2, 2017) periods  
134 from August 29, 2016 to February 2, 2017. To better understand the changes of atmospheric Hg  
135 concentrations in different periods, the WEC period was further divided into WEC1 (October 1 to  
136 December 30, 2016) and WEC2 (January 1 to February 2, 2017) periods. Lhasa is located in the  
137 central region and is the largest city on the Tibetan Plateau, covering an area of approximately 60  
138 km<sup>2</sup>. The Lhasa population in 2019 was 720,700, accounting for approximately 20.6% of the total  
139 population of the Tibet Autonomous Region (Tibet Bureau of Statistics, 2020). The entire city is in  
140 a flat river valley surrounded by mountains up to 5,500 m above sea level. During the ISM period  
141 (from May to September), the low pressure on the Tibetan Plateau attracts the summer monsoon  
142 from the Indian Ocean to the Plateau, exhibiting a wetter monsoon season (Qiu, 2008). During the  
143 non-monsoon season (from October to April), the large-scale atmospheric circulation on the Tibetan  
144 Plateau is mainly under the control of westerly winds, which largely come from the inland areas of  
145 Central Asia, presenting a drier season in Lhasa during this time (Huang et al., 2010; Guo et al.,  
146 2015). According to previous studies, the air quality in Lhasa may be influenced by local emissions  
147 from anthropogenic activities (e.g., power plants, cement facilities, vehicular traffic, and religious  
148 activities) (Li et al., 2008; Cong et al., 2011; Huang et al., 2010; Guo et al., 2015; Luo et al., 2016;  
149 Li et al., 2016a) and long-range transboundary atmospheric transport (Huang et al., 2016a; Huang  
150 et al., 2016b).



151

152 **Figure 1 Location of the Lhasa station in the Institute of Tibetan Plateau Research,**  
 153 **Chinese Academy of Sciences (red star).**

154

## 155 **2.2 GEM, GOM, and PBM active monitoring**

156 Monitoring in Lhasa was performed using Tekran models 2537 B, 1130, and 1135 (Tekran Inc.,  
 157 Toronto, Canada) for real-time continuous measurements of GEM, GOM, and PBM concentrations.  
 158 Model 2357b is the main analytical module used to analyze Hg concentrations employing the cold  
 159 atomic fluorescence technique. Model 1130 is divided into pump and lysimeter modules, which is  
 160 mainly used for the collection and resolution of GOM. Model 1135 is the particle collection module  
 161 that is mainly used to collect and analyze atmospheric Hg in the particulate state. During the actual  
 162 monitoring, considering the low air pressure on the Tibetan Plateau, we reduced the airflow of the  
 163 pump module to 7.5 L/min (Swartzendruber et al., 2009; Zhang et al., 2015a; Zhang et al., 2016;  
 164 Lin et al., 2019; Lin et al., 2022) and the airflow in model 2537B was reduced to 1 L/min to ensure  
 165 that atmospheric Hg monitoring could be continuously performed. All monitoring data were  
 166 converted to concentrations under standard atmospheric pressure. The Tekran 2537B analyzer was

167 automatically calibrated every 23 hours using the instrument's internal Hg permeation source and  
168 was calibrated before and after monitoring using an external Hg source. The same instrument setup  
169 was used for QNNP and Nyingchi (Lin et al., 2019; Lin et al., 2022). The Tekran ambient Hg  
170 analyzer has been described in detail in previous studies (Landis et al., 2002; Rutter et al. 2008; de  
171 Foy et al. 2016).

### 172 **2.3 Meteorological data and other pollutant data**

173 During the monitoring period, the Vantage Pro2 weather station (Davis Instruments, USA)  
174 recorded local temperature (accuracy of 0.1°C), relative humidity (accuracy of 1%), wind speed  
175 (accuracy of 0.1 m s<sup>-1</sup>), wind direction (accuracy of 1°), barometric pressure (accuracy of 0.1 hPa),  
176 solar radiation (accuracy of 1 W m<sup>-2</sup>), and UV index (accuracy 0.1 MEDs). Hourly measurements  
177 of PM<sub>2.5</sub>, PM<sub>10</sub>, SO<sub>2</sub>, NO<sub>2</sub>, O<sub>3</sub>, and CO concentrations and the air quality index (AQI) were obtained  
178 from monitoring stations hosted by the Ministry of Ecology and Environment of China and  
179 published by the China Environmental Monitoring Center. The station was set up 10 km from the  
180 atmospheric Hg monitoring station.

### 181 **2.4 Backward trajectory simulation and potential source analysis**

182 To better understand the transport paths of atmospheric GEM, the Hybrid Single-Particle  
183 Lagrangian Integrated Trajectory (HYSPPLIT) model was used to calculate backward trajectories  
184 (Stein et al., 2015; Chai et al., 2017; Chai et al., 2016; Hurst and Davis, 2017; Lin et al., 2019). The  
185 HYSPPLIT model (<https://www.arl.noaa.gov/hysplit/hysplit/>) is a hybrid approach that combines  
186 Lagrangian and Eulerian methods, which was developed by the National Oceanic and Atmospheric  
187 Administration (NOAA) as a tool to explain the transport, dispersion, and deposition of particles in  
188 the atmosphere. The backward trajectory simulation used Global Data Assimilation System (GDAS)  
189 data with 1°x1° latitude and longitude horizontal spatial resolution and 23 vertical heights every 6  
190 hours in this study. We examined the effect of arrival height on the trajectories using different arrival  
191 heights (50 m, 100 m, 400 m, and 1,000 m) in December 2016 (Figure S2). The results showed that  
192 the calculated trajectories of the air masses were almost the same when the arrival height was below  
193 400 m. The trajectory arrival altitude was then set to 100 m a.g.l in this study. The trajectories were  
194 computed every 6 hours with an inverse time of 120 hours. The trajectories could cover China,  
195 Nepal, India, Pakistan, and most of West Asia. Here, we combined the backward trajectory with

196 real-time Hg monitoring concentrations to represent the trajectories of GEM concentrations. Cluster  
197 analysis was performed after the trajectory calculation. Cluster analysis can indicate the main  
198 trajectory of incoming pathways and the GEM concentration indicated by the incoming trajectories.

## 199 **2.5 Principal component analysis**

200 Principal component analysis (PCA) is a data reduction method that allows a number of  
201 measured variables to be categorized into several factors that represent the behavior of the entire  
202 dataset (Jackson, 2005). In many previous Hg studies, PCA has been used to analyze the  
203 relationships between Hg and multiple pollutants and meteorological variables (Brooks et al., 2010;  
204 Cheng et al., 2012; Liu et al., 2007; Zhou et al., 2019; Lin et al., 2022). Prior to running the PCA,  
205 all variables were normalized by the standard deviation. To check whether PCA was the appropriate  
206 method for the dataset used in this study, Kaiser-Meyer-Olkin's measure of sampling adequacy  
207 (MSA>0.5) and Bartlett's Test of sphericity (P<0.05) tests were performed during data analysis.  
208 Total variance and rotated scree plots were used to determine the number of factors during the PCA  
209 analysis, and components with variance  $\geq 1.0$  were retained. Variables with high factor loadings  
210 (generally  $>0.5$ ) were identified as potential sources of Hg in this study.

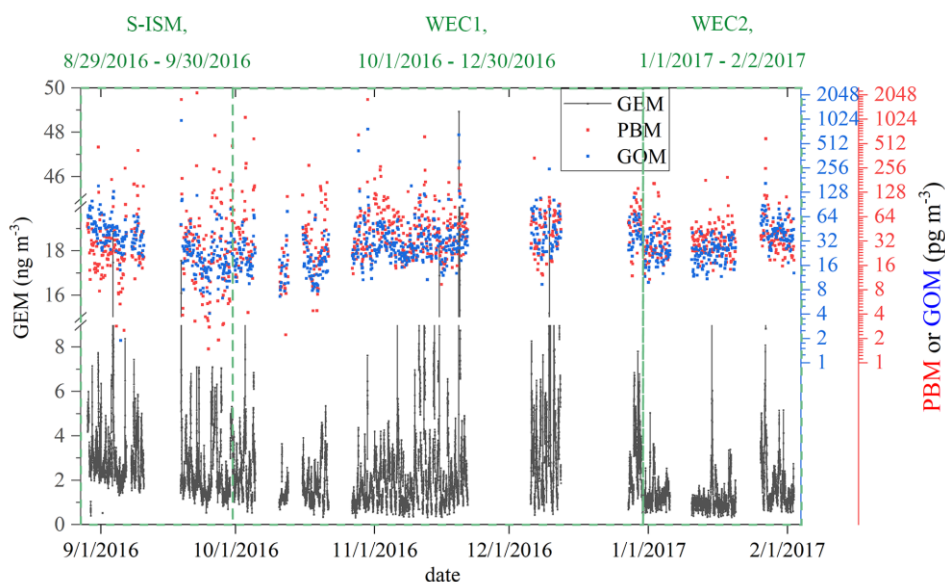
## 211 **3. Results and Discussion**

### 212 **3.1 Atmospheric Hg Monitoring in Lhasa**

213 Atmospheric Hg monitoring in Lhasa comprised the subsequent Indian Summer Monsoon (S-  
214 ISM) and Westerly circulation (WEC) periods from August 29, 2016 to February 2, 2017. Figure 2  
215 shows the variation in atmospheric Hg concentrations at the station during the monitoring period.  
216 During the whole monitoring period, the mean concentrations of GEM, GOM, and PBM at the  
217 station were  $2.26 \pm 1.97 \text{ ng m}^{-3}$ ,  $36.4 \pm 48.9 \text{ pg m}^{-3}$ , and  $54.5 \pm 119.5 \text{ pg m}^{-3}$  (mean concentration  $\pm$   
218 standard deviation), respectively. During the S-ISM period, the concentrations of GEM, GOM, and  
219 PBM were  $2.73 \pm 1.48 \text{ ng m}^{-3}$ ,  $38.4 \pm 62.7 \text{ pg m}^{-3}$ , and  $59.1 \pm 181.0 \text{ pg m}^{-3}$ , respectively. While during  
220 the WEC period, the concentrations of GEM, GOM, and PBM were  $2.11 \pm 2.09 \text{ ng m}^{-3}$ ,  $35.8 \pm 43.3$   
221  $\text{pg m}^{-3}$ , and  $52.9 \pm 90.1 \text{ pg m}^{-3}$ , respectively. The GEM concentrations during the S-ISM period were  
222 significantly higher than those during the WEC period ( $p < 0.01$ ), while the mean concentrations of  
223 GOM and PBM in the S-ISM period were slightly higher than those in the WEC period. Overall,  
224 GEM concentrations showed a decreasing trend throughout the monitoring period, with the average



225 weekly concentration decreasing from 3.21 ng m<sup>-3</sup> at the beginning of the monitoring period to 1.60  
 226 ng m<sup>-3</sup> at the end of the monitoring period, which is contrast to previous studies, which showed that  
 227 atmospheric Hg concentrations in the Northern Hemisphere is low in summer and high in winter  
 228 (Horowitz et al., 2017; Jiskra et al., 2018). The different variation trends between Lhasa and the  
 229 whole Northern Hemisphere may be related to the special location of Lhasa. Unexpectedly high  
 230 concentrations were found at irregular intervals for all Hg species. The occurrence time of these  
 231 high concentrations was random, and high GEM concentrations did not always occur at the same  
 232 time as high GOM or PBM concentrations, indicating the complexity of the Hg sources of the  
 233 species. For GOM and PBM, relatively comparable trends between them may be related to similar  
 234 sources, transport, and transformation reactions in the atmosphere.



235  
 236 **Figure 2 Time series of GEM, GOM, and PBM concentrations over the sampling period. The**  
 237 **GEM concentration resolution was 5 min and the GOM and PBM resolutions was 2 h.**  
 238

239 In early September, GOM concentrations were generally higher than PBM concentrations. In  
 240 the subsequent period, PBM concentrations were always higher than GOM concentrations, which  
 241 may indicate that the sources and composition of pollutants at this time were not consistent with  
 242 those in the latter period. GOM and PBM may undergo mutual transformation in the atmosphere,  
 243 which may be related to temperature, humidity, and atmospheric composition (Rutter and Schauer,  
 244 2007; Rutter et al., 2008), and thus the concentration distributions of GOM and PBM may also be

245 related to the changes of local climate and atmospheric composition from S-ISM to WEC periods.  
246 The GOM and PBM concentrations were higher in November and December. Since GOM and PBM  
247 are mainly from local emissions, the changes in their concentrations may indicate that there are  
248 more local sources at this period. As Lhasa enters the heating season in November-December, and  
249 there are more local religious activities at this time, there may be more local combustion sources.  
250 Table 1 lists the concentrations of Hg and other pollutants during the monitoring period. PM<sub>2.5</sub>  
251 concentration increased significantly in the WEC1 period, indicating the presence of more

252 particulate matter during this period. This could explain the elevated concentrations of GOM and

Table 1 Statistics metrics of species Hg, meteorological factors, and other pollutants

Period	Stat	GEM (ng m <sup>-3</sup> )	PBM (pg m <sup>-3</sup> )	GOM (pg m <sup>-3</sup> )	Temp (°C)	Hum. (%)	Wind speed (m s <sup>-1</sup> )	Solar radiation (W m <sup>-2</sup> )	CO (mg m <sup>-3</sup> )	NO <sub>2</sub> (µg m <sup>-3</sup> )	O <sub>3</sub> (µg m <sup>-3</sup> )	PM <sub>2.5</sub> (µg m <sup>-3</sup> )	SO <sub>2</sub> (µg m <sup>-3</sup> )
S-ISM	Mean	2.73	59.08	38.39	14.42	61.45	1.70	212.60	0.39	26.44	72.18	16.26	4.19
	SD	1.48	181.38	62.85	3.70	16.96	1.41	313.90	0.18	19.36	28.68	13.12	2.08
	Median	2.36	24.50	30.30	13.90	62.00	1.30	7.00	0.30	22.00	77.00	13.00	4.00
	Min	0.40	-11.44	1.89	5.90	14.00	0.00	0.00	0.10	1.00	1.00	1.00	1.00
	Max	18.87	2165.70	988.50	24.70	93.00	13.00	1290.00	1.70	110.00	133.00	81.00	21.00
WEC1	Mean	2.39	57.55	37.46	6.90	26.01	1.28	169.56	0.64	45.24	45.39	47.97	5.51
	SD	2.35	104.15	50.98	5.75	15.08	1.39	246.66	0.51	31.01	34.44	46.19	5.35
	Median	1.79	38.80	27.83	6.90	24.00	0.90	0.00	0.50	41.00	43.00	35.00	5.00
	Min	0.31	0.00	1.89	-6.20	1.00	0.00	0.00	0.10	2.00	1.00	1.00	1.00
	Max	48.93	1797.30	774.86	21.60	94.00	9.80	973.00	4.40	152.00	133.00	458.00	145.00
WEC2	Mean	1.47	42.82	32.05	0.22	25.59	1.97	123.61	0.56	26.78	65.22	23.73	4.49
	SD	1.12	45.39	17.14	3.98	14.67	1.85	186.98	0.30	22.61	26.30	18.77	2.61
	Median	1.17	33.77	27.50	0.20	24.00	1.30	0.00	0.50	19.00	71.00	19.00	4.00
	Min	0.33	0.00	9.91	-8.80	2.00	0.00	0.00	0.20	2.00	1.00	1.00	1.00
	Max	20.86	589.43	165.06	10.20	68.00	11.20	662.00	2.60	99.00	108.00	118.00	32.00

253 PBM from November-December.

254

255 Table 2 shows the distributions of atmospheric Hg concentrations in some provincial capitals  
 256 in China and nearby monitoring stations from literature. In general, the GEM concentration in Lhasa  
 257 is low among the provincial capitals in China. The GEM concentration in other provincial capitals

258 of China was approximately 3-10 ng m<sup>-3</sup>. Guiyang, Chongqing, and Lanzhou were the nearest  
259 provincial capitals to Lhasa, with GEM concentrations reported in the literature, all located in  
260 western China. Guiyang had a very high GEM concentration due to the presence of local Hg mines  
261 (Liu et al., 2011; Yang et al., 2009). The GEM concentration in Chongqing was approximately three  
262 times higher than that of Lhasa. The higher GEM concentration in Chongqing was likely due to its  
263 proximity to the Hg-contaminated area and large population (Yang et al., 2009). Compared to  
264 Lanzhou, another high-altitude city, the GEM concentration in Lhasa was approximately half that  
265 of Lanzhou, which may be owing to the overall cleaner environment with fewer local pollution  
266 sources in Lhasa (Yin et al., 2020a). The GOM and PBM concentrations in other provincial capitals  
267 were relatively less monitored. However, GOM concentrations in Lhasa were significantly higher  
268 than those in cities with GOM monitoring, such as mega-cities like Beijing and Shanghai, and even  
269 higher than those in Guiyang, where Hg mines are located. GOM concentrations in provincial  
270 capitals nationwide were mainly concentrated between 3-20 pg m<sup>-3</sup>, whereas the GOM  
271 concentrations in Lhasa were approximately 2-10 times higher than the average concentration in  
272 provincial capitals. The high GOM concentration in Lhasa is likely due to its high altitude. Lhasa is  
273 exposed to much higher solar radiation and has more ice surfaces than inland areas, which may have  
274 contributed to the oxidation of GEM or the re-release of GOM deposited in snow and ice (Steffen  
275 et al., 2008; Dommergue et al., 2003; Song et al., 2018). In contrast, the PBM concentration in Lhasa  
276 was at a lower level, only somewhat higher than that in Hefei. The monitoring period in Lhasa was  
277 mainly in winter when there were more particulate matter emissions than in summer owing to  
278 heating combustion. The PM<sub>2.5</sub> concentration in Lhasa was low throughout the monitoring period  
279 (Table 1), which indicated that the local particulate matter emissions were low; this may be the main  
280 reason for the low PBM concentration.

Table 2 Comparison of atmospheric Hg concentrations at some provincial capitals in China and some nearby monitoring stations

Location	altitude	type	region	Monitoring period	GEM (ng m <sup>-3</sup> )	GOM (pg m <sup>-3</sup> )	PBM (pg m <sup>-3</sup> )	GEM diurnal variation (local time/GEM concentration)			reference
								Peak (ng m <sup>-3</sup> )	Valley (ng m <sup>-3</sup> )	Variation (ng m <sup>-3</sup> )	
<b>Lhasa</b>	<b>3600</b>	<b>City</b>	<b>Southwest</b>	<b>8/2016-2/2017</b>	<b>2.26±1.97</b>	<b>36.4±48.9</b>	<b>54.5±119.5</b>				<b>This study</b>
Beijing	40	City	North china	12/2008-11/2009	3.22±1.74	10.1±18.8	98.2±112.7				(Zhang et al., 2013)
Hefei	30	City	East china	7/2013-6/2014	4.07±1.91	3.67±5.11	30.0±100.3				(Hong et al., 2016)
Shanghai	4	City	East china	2014	4.19±9.13	21±100	197±877				(Duan et al., 2017)
Lanzhou	1525	City	Northwest	10/2016-10/2017	4.48±2.32						(Yin et al., 2020a)
Jinan	148	City	East china	10/2015 -7/2016	4.91±3.66		451.9±433.4				(Li et al., 2017)
Chongqing	300	City	Southwest	2006-2007	6.74±0.37						(Yang et al., 2009)
Nanjing	25	City	East china	2011	7.9±7.0						(Zhu et al., 2012)
Guiyang	1150	City	Southwest	8/2009-12/2009	9.72±10.2	35.7±43.9	368±676				(Liu et al., 2011)
Ev-K2, Nepal	5050	Remote		11/2011-4/2012	1.2±0.2		18/1.30	6/1.10	0.20		(Gratz et al., 2013)
Nam Co, China	5300	Remote		11/2014-3/2015	1.33±0.24						(Yin et al., 2018)
Waliguan, China	3816	Remote		9/2007-9/2008	1.98±0.98	7.4±4.8	19.4±18.1	6/2.30	14/1.94	0.36	(Fu et al., 2012b)
Shangri-La, China	3580	Remote		11/2009-11/2010	2.51±0.73	8.22±7.9	38.32±31.26	17/2.48	6/1.71	0.77	(Zhang et al., 2015a)
Gongga, China	1640	Remote		5/2005-6/2006	3.98			11/4.45	2/3.55	0.90	(Fu et al., 2008)
QNNP, China	4267	Remote		4/2016-8/2016	1.42±0.37	21.4±13.4	25.6±19.1	6/2.04	13/1.11	0.93	(Lin et al., 2019)
Nyingchi, China	3263	Remote		3/2019-9/2019	1.01±0.27	12.8±13.3	9.3±5.9	20/1.07	6/0.96	0.11	(Lin et al., 2022)

282 Compared to nearby monitoring stations (Table 2), Hg species concentrations in Lhasa were  
283 high. Namco station is the nearest station; its altitude is 4,730 m and the distance between the two  
284 stations is approximately 120 km. The GEM concentration in Namco was  $1.33 \pm 0.24 \text{ ng m}^{-3}$ , which  
285 was only 59% of Lhasa. This is likely because the Namco region is sparsely populated with minimal  
286 local pollution and is far from major Hg pollution sources (Yin et al., 2018). Compared to the QNNP  
287 (Lin et al., 2019) on Mt. Everest, which is approximately 500 km apart, the GEM, GOM, and PBM  
288 concentrations in Lhasa were approximately 1.6, 1.7, and 2.1 times higher, respectively. Our  
289 previous studies demonstrated that the QNNP is influenced by transported air masses from the  
290 Indian subcontinent, indicating that the concentration in Lhasa is high in the Tibetan Plateau.  
291 Compared to another typical highland site, Nyingchi, Lhasa had much high levels of atmospheric  
292 Hg species, which may be related to the vegetation uptake effects and strong wet deposition in  
293 Nyingchi (Lin et al., 2022). Among the surrounding stations, only Mt. Gongga and Shangri-La  
294 stations had higher GEM concentrations than Lhasa. The GEM concentrations reported at Mt.  
295 Gongga station ranged from May 2005 to July 2006. Considering that the smelting activities near  
296 this site were crude at that time and there were almost no air pollution control measures, the high  
297 local GEM concentrations may be strongly affected by local smelting activities and fuel combustion  
298 (Fu et al., 2008). In contrast, GEM concentrations in the Shangri-La region were mainly controlled  
299 by the monsoon, and Zhang et al. (2015a) suggested that all local GEM above  $2.5 \text{ ng m}^{-3}$  are  
300 associated with the transport of dry air carrying domestic and foreign regional anthropogenic  
301 emissions. Comparing these sites only for the monsoon period, the GEM concentration in Lhasa  
302 was higher than that in the Shangri-La region. As for GOM and PBM, the concentrations at the  
303 Lhasa station were much higher than those in the surrounding areas. The average GOM  
304 concentration in the surrounding areas was approximately  $10 \text{ pg m}^{-3}$ , which was only 27% of that  
305 in Lhasa, and the average PBM concentration in the surrounding areas was approximately  $28 \text{ pg m}^{-3}$ ,  
306 which was only 54% of that in Lhasa. Considering that GOM and PBM are mainly from local or  
307 surrounding sources or atmospheric transport (Lindberg and Stratton, 1998; Seigneur et al., 2006;  
308 Lynam et al., 2014), high GOM and PBM concentrations may indicate additional local sources of  
309 Hg in Lhasa.

### 310 **3.2 Unexpected high concentration events in Lhasa**

311 To investigate the reasons for the random high atmospheric Hg concentration events in Lhasa,  
312 typical high-value occurrence processes (defined as GEM concentrations above  $10 \text{ ng m}^{-3}$  monitored  
313 more than five times on a single day) were selected for analysis in the S-ISM and WEC periods,  
314 respectively. A total of seven high GEM concentration events were identified, of which, September  
315 3, November 10, November 19, and December 9, 2016, were selected for analysis; September 18,  
316 October 3, 2016, and January 27, 2017 were omitted due to lack of meteorological data or Hg  
317 concentration data for the proximity date.

318 During the S-ISM period (Figure 2), there was a clear peak in Hg concentration on September  
319 3, while the GEM, GOM, and PBM concentrations were approximately 1.6, 1.5, and 2.3 times the  
320 average daily value, respectively. Comparing the two days before and after the high-concentration  
321 event (Table 3, Figure 3. a), the concentrations of the three pollutants  $\text{NO}_2/\text{PM}_{2.5}/\text{SO}_2$ , were higher  
322 on September 3. High GEM concentrations were accompanied by winds of  $2.12 \text{ m/s}$  from the  
323 southwest, with  $\text{NO}_2$  and  $\text{SO}_2$  concentrations higher than usual as well as increased PBM  
324 concentrations.  $\text{NO}_2$  and  $\text{SO}_2$  are typical combustion source pollutants, and the presence of  $\text{PM}_{2.5}$ ,  
325 and PBM may indicate more combustion sources in the day. Thus, it can be inferred that the elevated  
326 Hg concentration event on September 3 may have originated mainly from a combustion event  
327 nearby or further away.

328 During the WEC period, significantly high values were observed on November 10, November  
329 19, and December 9. On November 10 (Figure 3.b), the increase in atmospheric Hg species  
330 concentrations was accompanied by significant increases in  $\text{CO}/\text{NO}_2/\text{PM}_{10}/\text{PM}_{2.5}/\text{SO}_2$   
331 concentrations. Two similar peaks in atmospheric Hg species concentrations were also observed  
332 around November 10, with relatively lower peak concentrations. During these three events, the  
333 concentrations of other pollutants were higher than usual, whereas wind speeds were extremely low  
334 during the event periods. In addition, extremely high PBM concentrations ( $297.7 \pm 189.3 \text{ pg m}^{-3}$ ,  
335 maximum  $621.2 \text{ pg m}^{-3}$ ) were observed at midnight on November 12 which, considering the  
336 extremely low wind speed and the presence of a low height nocturnal boundary layer, may indicate  
337 that the high concentrations originated from local sources.

Table 3 Comparison of the pollutant concentrations with the two days before and after the high Hg concentration events

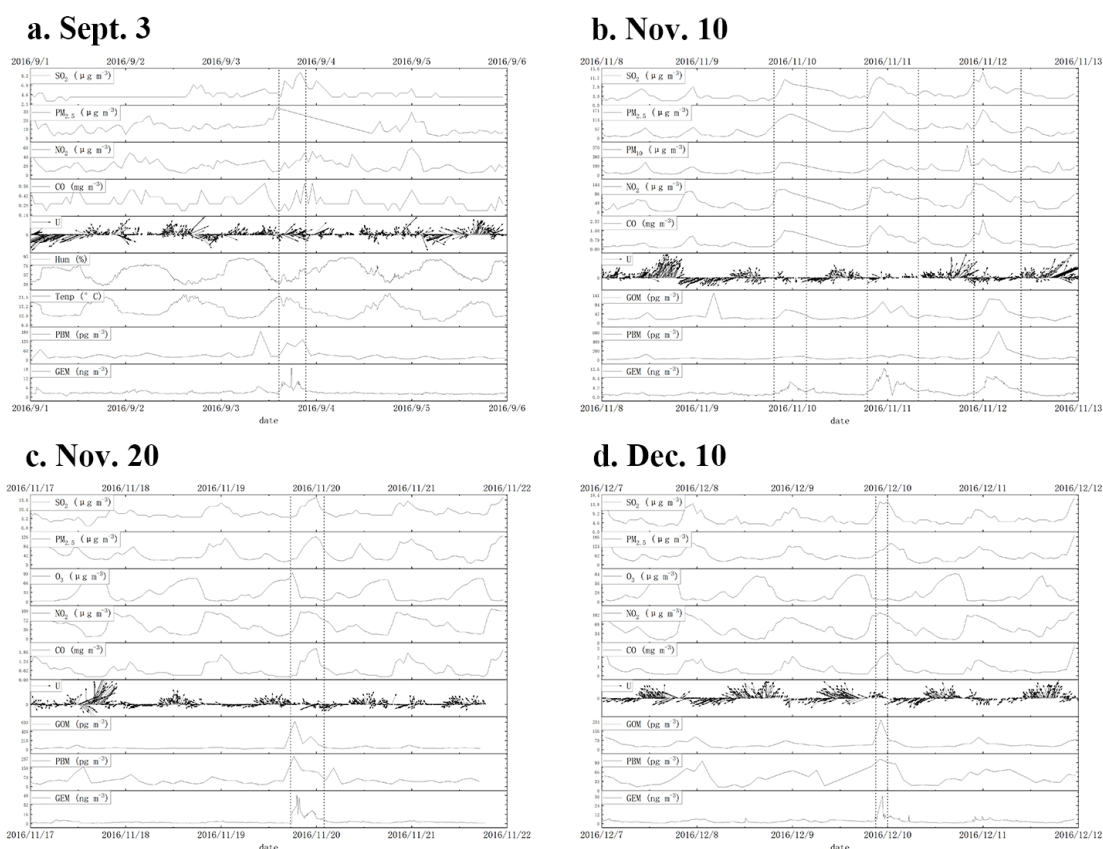
Item	9.1-2	9.3	9.4-5	11.8-9	11.10	11.11-12	11.17-18	11.19	11.20-21	12.7-8	12.10-11
GEM (ng m <sup>-3</sup> )	2.72	<b>4.63</b>	3.03	1.47	<b>3.16</b>	<b>2.96</b>	2.15	<b>6.87</b>	2.66	2.76	<b>5.43</b>
PBM (pg m <sup>-3</sup> )	25.32	<b>64.17</b>	31.52	36.31	<b>47.21</b>	<b>94.80</b>	53.41	<b>74.78</b>	55.40	38.71	<b>66.74</b>
GOM (pg m <sup>-3</sup> )	40.95	<b>63.84</b>	42.55	32.76	<b>39.48</b>	<b>42.03</b>	35.29	<b>119.39</b>	44.86	43.84	<b>69.65</b>
Temp. (°C)	16.61	15.86	15.32	7.06	7.76	8.80	4.20	4.49	4.94	3.13	2.88
Hum. (%)	58.47	67.89	68.71	19.96	22.02	21.04	21.82	23.35	25.67	23.50	26.86
Wind (m s <sup>-1</sup> )	2.37	1.46	1.49	1.47	<b>0.93</b>	1.17	1.05	<b>0.71</b>	0.75	0.88	0.89
Barometer (hPa)	651.62	651.08	652.39	654.90	654.33	652.31	655.11	652.18	653.57	657.99	655.66
rainfall (mm)	0.01	0.17	0.36	0.00	0.00	0.00	0.00	0.00	0.00	0.00	0.00
Solar Rad. (W m <sup>-2</sup> )	241.20	201.15	214.39	189.02	194.45	182.30	166.14	161.59	180.02	141.61	139.69
CO (mg m <sup>-3</sup> )	0.34	<b>0.36</b>	0.32	0.39	<b>0.76</b>	<b>0.63</b>	0.64	0.71	0.72	0.67	0.80
NO <sub>2</sub> (µg m <sup>-3</sup> )	20.44	<b>26.00</b>	21.77	41.38	<b>57.64</b>	<b>66.48</b>	54.58	53.58	55.27	48.87	55.33
O <sub>3</sub> (µg m <sup>-3</sup> )	85.73	77.42	72.56	59.27	57.43	49.46	34.73	34.79	29.51	31.37	28.38
PM <sub>10</sub> (µg m <sup>-3</sup> )	33.90	32.78	26.95	80.71	<b>130.07</b>	<b>155.44</b>	107.98	<b>119.79</b>	<b>146.29</b>	125.82	137.74
PM <sub>2.5</sub> (µg m <sup>-3</sup> )	11.98	<b>17.10</b>	10.98	31.20	<b>75.07</b>	<b>64.85</b>	51.21	50.13	53.83	62.80	65.46
SO <sub>2</sub> (µg m <sup>-3</sup> )	4.23	<b>5.89</b>	4.91	3.83	<b>6.07</b>	<b>5.71</b>	6.50	<b>8.92</b>	<b>9.44</b>	6.00	6.88

338

339 On November 19 (Figure 3.c), there was a significant increase in all atmospheric Hg species  
 340 concentrations. During the elevated period, the average GEM, GOM, and PBM concentrations were  
 341  $17.94 \pm 10.54$  ng m<sup>-3</sup>,  $302.5 \pm 218.5$  pg m<sup>-3</sup>, and  $162.4 \pm 54.0$  pg m<sup>-3</sup>, respectively, which were 8.3, 5.7,



342 and 4.6 times higher than the average concentrations on November 17-18. However, only a slight  
 343 increase in the peak CO/PM<sub>2.5</sub>/SO<sub>2</sub> concentration was observed during the event period. Therefore,  
 344 the increase in atmospheric Hg species concentrations may indicate that this event was unique, with  
 345 certain sources of high Hg concentrations. The low wind speed and low nocturnal boundary layer  
 346 height both contributed to the accumulation of atmospheric Hg species, which also indicated that  
 347 the elevated Hg was from local sources. Similar to the event on November 19, sharp increases in  
 348 atmospheric Hg species concentrations were observed only on December 9 (Figure 3.d). The  
 349 atmospheric Hg species concentration increase events during the WEC period occurred at night and,  
 350 given that it coincided with the winter heating period, local combustion sources may be the unique  
 351 sources that may contribute to the Hg concentration increase.

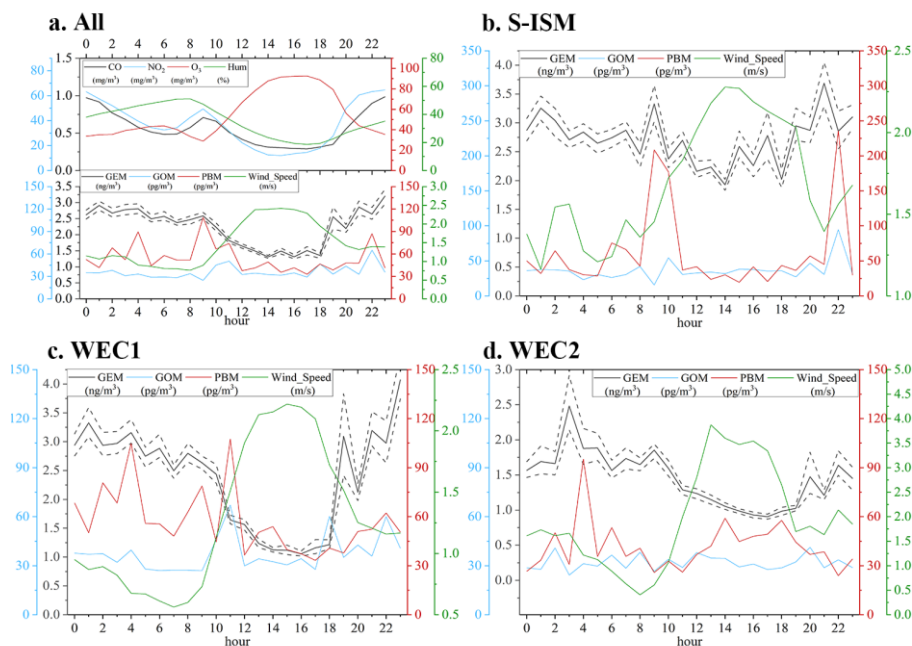


352  
 353 **Figure 3 Comparison of the pollutant concentrations with those at the two days before and**  
 354 **after the high Hg concentration events. The dotted lines indicate the area where the Hg**  
 355 **concentrations are significantly elevated**

356 **3.3 Diurnal variation of atmospheric Hg in Lhasa**

357 Figure 4.a shows the diurnal variation of atmospheric Hg in Lhasa during the monitoring period.

358 The mean GEM concentration during this period was  $2.26 \pm 1.97 \text{ ng m}^{-3}$ , and the maximum  
 359 difference of hourly average GEM diurnal variation was  $1.89 \text{ ng m}^{-3}$ . GEM concentration was low  
 360 during the day; the lowest concentration of the day appeared from 14:00-18:00 (UTC+8). The GEM  
 361 concentration kept increasing and reached the peak at midnight. During the night, the GEM  
 362 concentration maintained in high value with little dissipation. Subsequently, the GEM concentration  
 363 decreased rapidly with the sunrise. Overall, the diurnal variation of GEM concentration was similar  
 364 to CO, NO<sub>2</sub>, and relative humidity, and opposite to O<sub>3</sub> and wind speed. The high GEM  
 365 concentrations at night can be attributed to the lower boundary layer height at night (average at 131  
 366 m a.g.l. during the observation period, between 19:00 and 07:00, UTC+8) and the lower wind speed  
 367 (Figure 4). Also, the average night temperature in Lhasa during the monitoring period was 5.8°C,  
 368 and the residents heating combustion may bring about the release of GEM. After sunrise, the  
 369 boundary layer height increased rapidly and the diffusion quickly occurred in the lower atmosphere.  
 370 During the increase of wind speed, airflows were carried from other regions with few populations,  
 371 which may lead to a decrease in GEM concentrations. For both GOM and PBM, the higher GOM  
 372 concentrations occurred during the day and higher PBM concentration occurred during the night.  
 373 No obvious increase occurred for GOM and PBM concentrations at the same time, which may  
 374 indicate that there is no local common external source, and the variation of GOM and PBM  
 375 concentrations may come from the gas-particle redistribution process of atmospheric Hg(II).



376

377 **Figure 4 Diurnal variations of Hg species, concentrations of other pollutants, and**  
378 **meteorological information from S-ISM to WEC periods. The short horizontal line**  
379 **represents the concentration error range for each time period.**

380 In particular, during the S-ISM period (Figure 4.b), the diurnal variation in GEM  
381 concentrations fluctuated frequently, which indicates that the factors affecting the concentration  
382 variation were very complicated. The mean concentration of GEM during this period was 2.73 ng  
383 m<sup>-3</sup>, and the maximum difference of GEM diurnal variation was 1.40 ng m<sup>-3</sup>. September was the  
384 ending period of the Indian summer monsoon, and the external transboundary transport of air masses  
385 by the monsoon may have been weakened. Simultaneously, the average temperature in September  
386 was high (14.4°C) without residents heating during the night, which may be the reason for the small  
387 diurnal variation in GEM concentrations. Overall, GEM concentrations remained lower during the  
388 day, increased, and remained high at night. No clear pattern of variation was observed in GOM and  
389 PBM during this period.

390 During the WEC1 period, the diurnal variation in GEM concentrations was exceedingly large.  
391 The mean GEM value was 2.39 ng m<sup>-3</sup> with great GEM diurnal variation value (3.01 ng m<sup>-3</sup>). The  
392 diurnal trend was roughly the same as the whole monitoring period, but the lowest value was 1.06  
393 ng m<sup>-3</sup> and the highest value was 4.07 ng m<sup>-3</sup>. The increase in night concentrations may be related  
394 to the beginning of the heating season, whereas the burning of yak dung, firewood, or other fuels  
395 for residential heating may release GEM and PBM, and accumulate within the boundary layer at  
396 night, leading to higher GEM concentrations (Rhode et al., 2007; Xiao et al., 2015; Chen et al.,  
397 2015). In contrast, low day values may be related to the wind field. Although the wind speed during  
398 the WEC1 period was similar to that during the S-ISM period, westerly circulation was prevalent in  
399 Lhasa during the WEC1 period, with air masses coming from the sparsely populated area with lower  
400 GEM concentrations. The westerly winds carry away the locally accumulated GEM air masses in  
401 Lhasa and bring in low GEM concentration air masses from west of Lhasa. During this period, the  
402 diurnal variation in GOM concentrations was not clear.

403 The influence of wind flow was evident during the WEC2 period. During this period, GEM  
404 concentrations in Lhasa were the lowest and close to 1.00 ng m<sup>-3</sup> in the late afternoon when wind  
405 speeds were the highest. Nighttime concentrations were lower in the WEC2 period than in the

406 WEC1 period, probably because wind speeds were also high at night during the WEC2 period  
407 (19:00-4:00 UTC+8, mean wind speed 1.74 m/s). The heating season was still in progress during  
408 the WEC2 period, but GEM emissions from heating were likely carried away by the continuous  
409 flow of air masses. Therefore, the mean GEM concentration in Lhasa during the winter was likely  
410 strongly influenced by wind speed.

411 Compared to the diurnal variation patterns obtained from monitoring in other remote areas of  
412 China (Figure S3), the diurnal variation of GEM in Lhasa is more unique, and a wide diurnal  
413 variation in concentration was observed. Valleys of GEM concentrations in the afternoon were also  
414 observed in Waliguan and Namco, but the concentration variation ranges were small in both areas.  
415 This could be related to the regional characteristics of the three sites. Waliguan is located in a  
416 mountainous area with no significant local anthropogenic sources, and is mainly influenced by  
417 valley winds (Fu et al., 2012b). Namco is located in the central Tibetan region away from  
418 anthropogenic sources. Although the wind speed was also high in the afternoon in Namco (Yin et  
419 al., 2018), it is likely that the diurnal variation in atmospheric GEM concentrations was small  
420 because the atmosphere was well-proportioned and there were no local sources; therefore, the  
421 changes in wind speed might not affect the GEM concentration. In contrast, with the difference in  
422 GEM concentrations between Lhasa and the transmitted external air mass, wind speed could  
423 significantly influence the GEM concentrations in Lhasa. Meteorological conditions may have  
424 played a more important role. We conjecture that the high nighttime concentrations in Lhasa may  
425 originate mainly from local emissions, while the high wind speed and mixing of clean external air  
426 masses in the afternoon reduce the local GEM concentrations.

#### 427 **3.4 Analysis of factors affecting atmospheric Hg concentration in Lhasa**

428 Overall, four principal components were obtained for each period, from S-ISM to WEC2, using  
429 PCA analyze, to analyze the relationships between Hg and multiple pollutants and meteorological  
430 variables. The Hg monitoring data, meteorological factors, and pollutant data in Lhasa were  
431 statistically and dimensionally reduced by PCA to analyze the relationships among them. The  
432 components related to Hg were selected and analyzed separately for each period, and the principal  
433 components were extracted (Table 4). According to the variable's loadings on each component, they  
434 were assigned as Special Hg-related factor, Local emission factor, and Wind factor.

Table 4 PCA factor loadings (varimax rotated factor matrix) for Hg in Lhasa, China.

Tentative Identification	Special Hg-related			Local emission		Wind	
	S-ISM	WEC1	WEC2	WEC1	WEC2	S-ISM	WEC2
preiod							
GEM	<b>0.87</b>	<b>0.63</b>	<b>0.9</b>	0.44	0.3	-0.21	-0.13
PBM	<b>0.96</b>	<b>0.79</b>	<b>0.63</b>				
GOM	<b>0.95</b>	<b>0.87</b>	<b>0.95</b>	0.11	0.1		
Temp				-0.29	0.2		<b>0.92</b>
Hum		-0.19	0.17	-0.26	-0.18	-0.26	<b>-0.75</b>
Wind_Speed	-0.1	-0.14		-0.37		<b>0.87</b>	<b>0.91</b>
Rain							
Solar_Rad.				-0.21			
CO	0.17		0.11	<b>0.87</b>	<b>0.69</b>	-0.22	<b>0.51</b>
NO <sub>2</sub>		0.13		<b>0.92</b>	<b>0.96</b>	-0.25	
O <sub>3</sub>			-0.36	<b>-0.89</b>	<b>-0.83</b>	<b>0.53</b>	
PM <sub>10</sub>	-0.14			<b>0.86</b>	<b>0.69</b>		0.14
PM <sub>2.5</sub>	-0.16		0.16	<b>0.83</b>	<b>0.86</b>		
SO <sub>2</sub>	0.26	0.17	<b>0.86</b>	<b>0.75</b>			
Variance Explained	19.6	13.69	21.88	35.13	24.94	9.25	18.32

Note: variables with high factor loadings (> 0.5) were marked in bold. For readability, variables with very low factor loadings (< 0.1) are not presented.

435

436 A special Hg-related factor (Factor 1) was assigned owing to the continuous high positive  
 437 loading of GEM, GOM, and PBM from the SISM to the WEC periods; only high positive loading  
 438 of SO<sub>2</sub> was found in the WEC2 period. For this factor, there was no significant relationship with  
 439 any other meteorological factors or pollutants. The high positive loading of this factor for all three  
 440 Hg species and the low correlation with meteorological factors and other pollutants may indicate  
 441 that this is a specific source of Hg. As the short transmission distance of the GOM and PBM, the  
 442 special Hg-related source should be closer to Lhasa. However, no particular source of Hg around  
 443 Lhasa has been reported in the literature, so the source indicated by this factor remains unclear.

444 Factor 2 had slight positive relationship with GEM and GOM, high positive loading of  
 445 CO/NO<sub>2</sub>/PM<sub>10</sub>/PM<sub>2.5</sub>/SO<sub>2</sub>, and high negative loading of O<sub>3</sub> during the WEC period. The high  
 446 positive loadings of CO/NO<sub>2</sub>/PM<sub>10</sub>/PM<sub>2.5</sub>/SO<sub>2</sub> may indicate that this factor is highly correlated with  
 447 the combustion source. As O<sub>3</sub> concentration rapidly decreased after sunset (Figure 4. a), high  
 448 negative loading of O<sub>3</sub> further indicated that this factor represented events during the nighttime with

449 low O<sub>3</sub> concentrations. Since the WEC period overlapped with the heating season in Lhasa, Factor  
450 2 may be strongly associated with heating combustion.

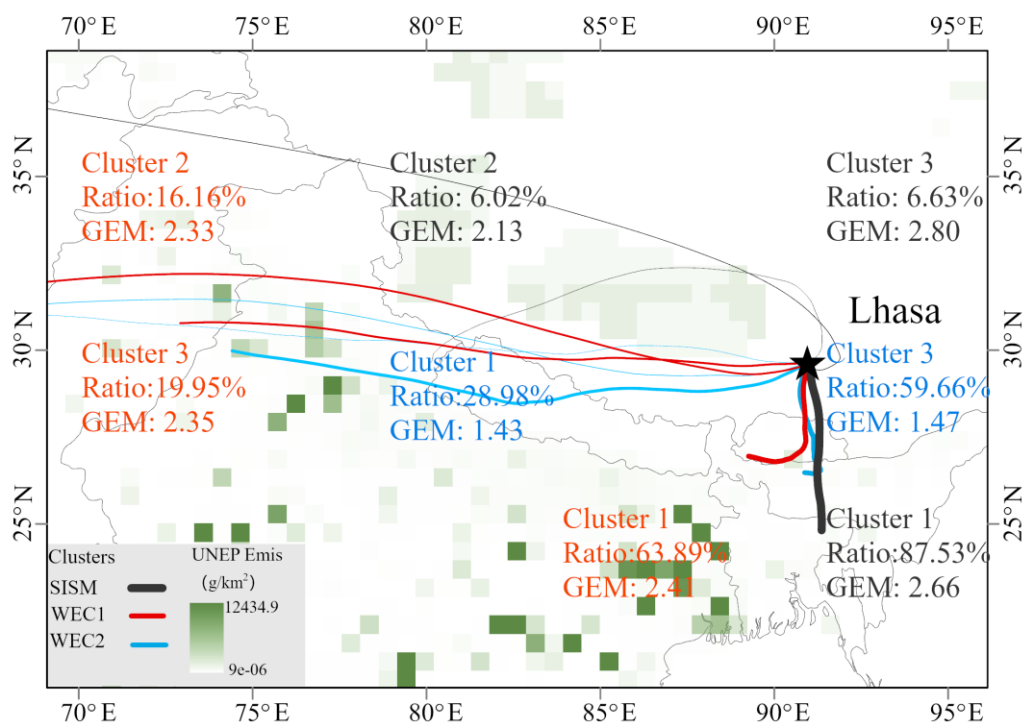
451 The wind factor (Factor 3) involves high positive loading of wind speed and low negative  
452 loading of GEM concentration during the S-ISM and WEC2 periods. This factor reveals the  
453 scavenging effect of wind on the local GEM in Lhasa. For high wind speed, the air masses with low  
454 GEM concentrations in the surrounding area mixed with the air masses in Lhasa, leading to a  
455 reduction in the GEM concentration. Concurrently, some GEM in Lhasa was carried away from the  
456 city by wind. At wind speed greater than 4m s<sup>-1</sup>, the average GEM concentration in Lhasa was  
457 1.31±0.93 ng m<sup>-3</sup>, which is similar to the average concentration of Nam Co (1.33±0.24 ng m<sup>-3</sup>) in  
458 the Tibetan hinterland. Factor 3 was consistent with the analysis of the wind effect on the diurnal  
459 variation of Hg concentrations (Section 3.2), indicating the effect of strong winds on urban Hg  
460 removal.

### 461 **3.5 Atmospheric Hg source trajectories and potential source regions in the Lhasa area**

462 Figure 4 shows the GEM backward trajectory paths from the S-ISM period to the WEC2 period  
463 in Lhasa. During the S-ISM period, most trajectories (cluster 1, representative GEM concentration  
464 of 2.66 ng m<sup>-3</sup>, 87.53% of the trajectory during this period, Table S1) originated from or passed  
465 through the south of Lhasa. The source of the trajectory points directly to the Indian Ocean, likely  
466 as these transported air masses are still subject to Indian monsoon action in September. According  
467 to the UNEP Hg emission inventory (Unep, 2013), there are few anthropogenic emissions along this  
468 trajectory, indicating that the GEM may originate from the Indian Ocean or locally from Lhasa.  
469 Clusters 2 and 3 may indicate the trajectories of air masses driven by westerly circulation, which  
470 had a low proportion in the S-ISM period, with slightly different GEM concentrations from different  
471 sources.

472 During the WEC1 period, the driving factor of the air mass gradually shifted from Indian  
473 monsoon to westerly circulation. Clusters 2 and 3 are trajectories driven by the higher-height  
474 westerly circulation during the WEC1 period with a higher proportion than in the S-ISM period.  
475 Cluster 1 came from the southwest of Lhasa, and the air mass moved along the Himalayas before  
476 entering the Tibetan Plateau and was transported to Lhasa. Compared to the S-ISM period, the GEM  
477 concentration of this trajectory decreased slightly, which may be related to the source of the air mass

478 and the areas it passes through. WEC2 showed little change in trajectory sources compared to WEC1,  
 479 but all trajectory concentrations decreased significantly. Both WEC1 and WEC2 were in winter,  
 480 and both had similar trajectories related to the driving wind field. Significantly decreasing GEM  
 481 concentrations may suggest a local influence in Lhasa City. The local GEM in Lhasa consists of  
 482 background concentrations superimposed on local emissions, and the share of local emissions  
 483 decreases under better dispersion conditions (higher wind speeds) during the WEC2 period. The  
 484 GEM concentration during the WEC2 period in Lhasa was only  $0.16 \text{ ng m}^{-3}$  higher than that during  
 485 the WEC period in the QNNP region ( $1.31 \pm 0.42 \text{ ng m}^{-3}$ ) (Lin et al., 2019)).  
 486



487 **Figure 5 Clusters of the back trajectory analysis from Lhasa during S-ISM and WEC**  
 488 **periods. The thickness of the line represents the ratio of the cluster in the time period, the**  
 489 **background is the global Hg emission inventory developed by UNEP (2013a).**

### 490 3.6 Comparison of three typical sites on the Tibetan Plateau

491 Different levels and variation patterns of Hg species concentrations were observed in the  
 492 Qomolangma National Nature Preserve (QNNP, 4,276 m) (Lin et al., 2019), Nyingchi (SET, 3,263  
 493 m) (Lin et al., 2022), and Lhasa (3,650 m) areas, which are typical monsoon-influenced, canyon,  
 494 and urban areas on the Tibetan Plateau, respectively. Predictably, Hg species concentrations were

495 generally lower on the Tibetan Plateau, while background areas with few populations on the Plateau  
496 were lower than those on the plains in mainland China, and cities on the Plateau were lower than  
497 those on the plains. Although the transboundary transport of pollutants has received considerable  
498 notice (Huang et al., 2016b; Wang et al., 2018; Lin et al., 2019; Zhu et al., 2019; Feng et al., 2019),  
499 the comparison between QNNP and Lhasa indicates that the contribution of local anthropogenic  
500 sources may be significant for atmospheric pollutant concentrations. The comparison also suggests  
501 that atmospheric Hg emissions from urban residential life may be an important source that can be  
502 valuable in inventory studies.

503 Vastly different patterns of Hg species concentrations were found in the QNNP and SET due  
504 to differences in geography and vegetation cover. Atmospheric Hg transported to QNNP is subject  
505 to a combination of monsoonal action and the pumping effect of glacial winds. However,  
506 atmospheric Hg entering the SET area has a slow elevation increasing path, and abundant  
507 precipitation and vegetation have a significant trapping effect on atmospheric Hg. While for Lhasa,  
508 a direct effect of local wind fields on the accumulation or rapid removal of GEM concentrations  
509 was found. This suggests that although global transport is important in the Hg cycle, the pollution  
510 at each location is likely to be strongly influenced by the local environment, even in exceptionally  
511 clean areas such as the Tibetan Plateau. However, there are still relatively few studies on GOM and  
512 PBM in the Tibetan Plateau, and more comprehensive investigations are required on how changes  
513 in Hg speciation transformation on snow and ice surfaces affect the environment, the effect of  
514 stratospheric intrusion on GOM concentrations (which is common on the Plateau), and the effect of  
515 particulate matter on Hg(II) gas-particle partitioning, which would help to understand the Hg species  
516 change on the Plateau and throughout the world.

#### 517 **4. Conclusions**

518 Lhasa is the largest city on the Tibetan Plateau; thus, its atmospheric Hg concentrations  
519 represent the highest level of atmospheric Hg pollution in this area. Unexpectedly high  
520 concentrations of atmospheric Hg species were found in Lhasa. The GEM concentrations were  
521 higher than the Northern Hemisphere background concentrations, and the GOM and PBM  
522 concentrations were high among Chinese cities. Monitoring of atmospheric Hg in Lhasa showed  
523 that the mean concentrations of GEM, GOM, and PBM during the S-ISM period ( $2.73 \pm 1.48 \text{ ng m}^{-3}$ )



524 <sup>3</sup>,  $38.4 \pm 62.7 \text{ pg m}^{-3}$ , and  $59.1 \pm 181.0 \text{ pg m}^{-3}$ , respectively) were higher than those during the WEC  
525 period ( $2.11 \pm 2.09 \text{ ng m}^{-3}$ ,  $35.8 \pm 43.3 \text{ pg m}^{-3}$ , and  $52.9 \pm 90.1 \text{ pg m}^{-3}$ , respectively). Combined  
526 with the trajectory analysis, the high atmospheric Hg concentrations during the S-ISM phase may  
527 have originated from external long-range transport.

528 Analysis of the overall concentration changes revealed some irregular and sudden high  
529 atmospheric Hg concentration events in Lhasa. Analysis of these events suggests that local sources  
530 (such as combustion events) can cause severely elevated concentration events under low wind  
531 speeds and the presence of a low-height nighttime boundary layer. Analysis of the diurnal variation  
532 of concentrations confirmed that low wind speeds and a low height nocturnal boundary layer would  
533 lead to the elevated local Hg concentrations. In contrast, higher wind speeds could rapidly remove  
534 atmospheric Hg from Lhasa. PCA analysis of the influencing factors indicates that local sources,  
535 especially special Hg-related sources, are important factors influencing the variability of  
536 atmospheric Hg. The PCA analysis also indicated the important role of higher wind speeds in  
537 reducing atmospheric Hg concentrations in the urban areas of Lhasa, likely owing to the large Hg  
538 concentration difference between Lhasa and surrounding areas.

539 Up to this study, we have obtained atmospheric Hg monitoring data from four typical areas of  
540 the Tibetan Plateau: Lhasa, QNNP, SET, and Namco. The atmospheric Hg concentrations in the  
541 background areas were at or below the average GEM concentration of Northern Hemisphere, with  
542 higher levels in the urban area of Lhasa. Factors such as long-range transport of atmospheric Hg,  
543 effects of local meteorological conditions, local glaciers, etc., were considered in these studies.  
544 Further monitoring of additional areas and regional simulations are required to confirm the  
545 atmospheric Hg transport patterns and fluxes.

546

#### 547 **Acknowledgments**

548 This study was funded by the National Natural Science Foundation of China (Grant #41821005,  
549 41977311, 42122059, 41907328). The authors are grateful to NOAA for providing the HYSPLIT  
550 model and GFS meteorological files. We also thank the staffs of Lhasa station of the Institute of  
551 Tibetan Plateau Research, Chinese Academy of Sciences on Lhasa for field sampling assistance.

552 **Data availability.** All the data presented in this paper can be made available for scientific

553 purposes upon request to the corresponding authors.

554 **Author contributions.** HL,XW, YT, QZ and XY designed the research and performed field  
555 measurements. HL and YT performed the data analysis and model simulations. HL led the paper  
556 writing. LC,CY, ZC, QZ, SK, JL, JS and BF contributed to the scientific discussion and the paper  
557 preparation.

558 **Competing interests.** The authors declare that they have no conflict of interest.

559

560 **References**

- 561 Brooks, S., Luke, W., Cohen, M., Kelly, P., Lefer, B., and Rappenglück, B. J. A. E.: Mercury species  
562 measured atop the Moody Tower TRAMP site, Houston, Texas, 44, 4045-4055, 2010.
- 563 Chai, T., Stein, A., Ngan, F., and Draxler, R.: Inverse modeling with HYSPLIT Lagrangian Dispersion  
564 Model-Tests and Evaluation using the Cross Appalachian Tracer Experiment (CAPTEX) data, AGU  
565 Fall Meeting Abstracts,
- 566 Chai, T., Crawford, A., Stunder, B., Pavolonis, M. J., Draxler, R., and Stein, A.: Improving volcanic ash  
567 predictions with the HYSPLIT dispersion model by assimilating MODIS satellite retrievals,  
568 Atmospheric Chemistry and Physics, 17, 2865-2879, 2017.
- 569 Chen, P., Kang, S., Bai, J., Sillanpää, M., and Li, C.: Yak dung combustion aerosols in the Tibetan  
570 Plateau: Chemical characteristics and influence on the local atmospheric environment,  
571 Atmospheric Research, 156, 58-66, 10.1016/j.atmosres.2015.01.001, 2015.
- 572 Cheng, I., Zhang, L., Blanchard, P., Graydon, J., St Louis, V. J. A. C., and Physics: Source-receptor  
573 relationships for speciated atmospheric mercury at the remote Experimental Lakes Area,  
574 northwestern Ontario, Canada, 12, 1903-1922, 2012.
- 575 Ci, Z., Zhang, X., Wang, Z., and Niu, Z.: Atmospheric gaseous elemental mercury (GEM) over a  
576 coastal/rural site downwind of East China: temporal variation and long-range transport,  
577 Atmospheric Environment, 45, 2480-2487, 2011.
- 578 Cong, Z., Kang, S., Luo, C., Li, Q., Huang, J., Gao, S., and Li, X.: Trace elements and lead isotopic  
579 composition of PM10 in Lhasa, Tibet, Atmospheric Environment, 45, 6210-6215, 2011.
- 580 Dommergue, A., Ferrari, C. P., Gauchard, P. A., Boutron, C. F., Poissant, L., Pilote, M., Jitaru, P., and  
581 Adams, F. C. J. G. r. l.: The fate of mercury species in a sub-arctic snowpack during snowmelt, 30,  
582 2003.
- 583 Duan, L., Wang, X., Wang, D., Duan, Y., Cheng, N., and Xiu, G.: Atmospheric mercury speciation in  
584 Shanghai, China, Science of the Total Environment, 578, 460-468, 2017.
- 585 Feng, X. and Fu, X.: Monsoon-facilitated characteristics and transport of atmospheric mercury at  
586 a high-altitude background site in southwestern China, Atmos. Chem. Phys, 1680, 7324, 2016.
- 587 Feng, X., Fu, X., and Zhang, H.: Observations of atmospheric Hg species and depositions in remote  
588 areas of China, E3S Web of Conferences,
- 589 Feng, Y., Wang, W., and Liu, J. J. W.: Dilemmas in and Pathways to Transboundary Water  
590 Cooperation between China and India on the Yaluzangbu-Brahmaputra River, 11, 2096, 2019.
- 591 Fu, X., Feng, X., Sommar, J., and Wang, S.: A review of studies on atmospheric mercury in China,  
592 Science of the Total Environment, 421, 73-81, 2012a.
- 593 Fu, X., Feng, X., Zhu, W., Wang, S., and Lu, J.: Total gaseous mercury concentrations in ambient air  
594 in the eastern slope of Mt. Gongga, South-Eastern fringe of the Tibetan plateau, China,  
595 Atmospheric Environment, 42, 970-979, 2008.
- 596 Fu, X., Feng, X., Liang, P., Zhang, H., Ji, J., and Liu, P.: Temporal trend and sources of speciated  
597 atmospheric mercury at Waliguan GAW station, Northwestern China, Atmospheric Chemistry and  
598 Physics, 12, 1951-1964, 2012b.
- 599 Fu, X., Maruszczak, N., Heimbürger, L.-E., Sauvage, B., Gheusi, F., Prestbo, E. M., and Sonke, J. E.:  
600 Atmospheric mercury speciation dynamics at the high-altitude Pic du Midi Observatory, southern  
601 France, Atmos. Chem. Phys, 16, 5623-5639, 2016a.
- 602 Fu, X., Zhang, H., Feng, X., Tan, Q., Ming, L., Liu, C., Zhang, L. J. E. s., and technology: Domestic and  
603 transboundary sources of atmospheric particulate bound mercury in remote areas of China:

604 evidence from mercury isotopes, 53, 1947-1957, 2019.

605 Fu, X., Zhu, W., Zhang, H., Sommar, J., Yu, B., Yang, X., Wang, X., Lin, C.-J., and Feng, X.: Depletion  
606 of atmospheric gaseous elemental mercury by plant uptake at Mt. Changbai, Northeast China,  
607 Atmospheric Chemistry and Physics, 16, 12861-12873, 2016b.

608 Gay, D. A., Schmeltz, D., Prestbo, E., Olson, M., Sharac, T., and Tordon, R.: The Atmospheric Mercury  
609 Network: measurement and initial examination of an ongoing atmospheric mercury record across  
610 North America, Atmospheric Chemistry and Physics, 13, 11339-11349, 10.5194/acp-13-11339-  
611 2013, 2013.

612 Gratz, L., Esposito, G., Dalla Torre, S., Cofone, F., Pirrone, N., and Sprovieri, F.: First Measurements  
613 of Ambient Total Gaseous Mercury (TGM) at the EvK2CNR Pyramid Observatory in Nepal, E3S Web  
614 of Conferences,

615 Guo, J., Kang, S., Huang, J., Zhang, Q., Tripathee, L., and Sillanpää, M.: Seasonal variations of trace  
616 elements in precipitation at the largest city in Tibet, Lhasa, Atmospheric Research, 153, 87-97,  
617 2015.

618 Hong, Q., Xie, Z., Liu, C., Wang, F., Xie, P., Kang, H., Xu, J., Wang, J., Wu, F., and He, P.: Speciated  
619 atmospheric mercury on haze and non-haze days in an inland city in China, Atmospheric  
620 Chemistry and Physics, 16, 13807-13821, 2016.

621 Horowitz, H. M., Jacob, D. J., Zhang, Y., Dibble, T. S., Slemr, F., Amos, H. M., Schmidt, J. A., Corbitt,  
622 E. S., Marais, E. A., and Sunderland, E. M.: A new mechanism for atmospheric mercury redox  
623 chemistry: Implications for the global mercury budget, Atmospheric Chemistry and Physics, 17,  
624 6353-6371, 2017.

625 Hu, Q. H., Kang, H., Li, Z., Wang, Y. S., Ye, P. P., Zhang, L. L., Yu, J., Yu, X. W., Sun, C., and Xie, Z. Q.:  
626 Characterization of atmospheric mercury at a suburban site of central China from wintertime to  
627 springtime, Atmospheric Pollution Research, 5, 769-778, 2014.

628 Huang, J., Kang, S., Shen, C., Cong, Z., Liu, K., Wang, W., and Liu, L.: Seasonal variations and sources  
629 of ambient fossil and biogenic-derived carbonaceous aerosols based on <sup>14</sup>C measurements in  
630 Lhasa, Tibet, Atmospheric Research, 96, 553-559, 2010.

631 Huang, J., Kang, S., Guo, J., Zhang, Q., Cong, Z., Sillanpää, M., Zhang, G., Sun, S., and Tripathee, L.:  
632 Atmospheric particulate mercury in Lhasa city, Tibetan Plateau, Atmospheric Environment, 142,  
633 433-441, 2016a.

634 Huang, J., Kang, S., Tian, L., Guo, J., Zhang, Q., Cong, Z., Sillanpää, M., Sun, S., and Tripathee, L.:  
635 Influence of long-range transboundary transport on atmospheric water vapor mercury collected  
636 at the largest city of Tibet, Science of The Total Environment, 566, 1215-1222, 2016b.

637 Huang, J., Kang, S., Wang, S., Wang, L., Zhang, Q., Guo, J., Wang, K., Zhang, G., and Tripathee, L.:  
638 Wet deposition of mercury at Lhasa, the capital city of Tibet, Science of the total environment, 447,  
639 123-132, 2013.

640 Hurst, T. and Davis, C.: Forecasting volcanic ash deposition using HYSPLIT, Journal of Applied  
641 Volcanology, 6, 5, 2017.

642 Jackson, J. E.: A user's guide to principal components, John Wiley & Sons 2005.

643 Jiskra, M., Sonke, J. E., Obrist, D., Bieser, J., Ebinghaus, R., Myhre, C. L., Pfaffhuber, K. A., Wängberg,  
644 I., Kyllönen, K., and Worthy, D.: A vegetation control on seasonal variations in global atmospheric  
645 mercury concentrations, Nature Geoscience, 11, 244-250, 2018.

646 Kellerhals, M., Beauchamp, S., Belzer, W., Blanchard, P., Froude, F., Harvey, B., McDonald, K., Pilote,  
647 M., Poissant, L., and Puckett, K.: Temporal and spatial variability of total gaseous mercury in Canada:

648 results from the Canadian Atmospheric Mercury Measurement Network (CAMNet), *Atmospheric*  
649 *Environment*, 37, 1003-1011, 2003.

650 Lan, X., Talbot, R., Castro, M., Perry, K., and Luke, W.: Seasonal and diurnal variations of atmospheric  
651 mercury across the US determined from AMNet monitoring data, *Atmospheric Chemistry and*  
652 *Physics*, 12, 10569-10582, 2012.

653 Li, C., Chen, P., Kang, S., Yan, F., Hu, Z., Qu, B., and Sillanpää, M.: Concentrations and light  
654 absorption characteristics of carbonaceous aerosol in PM<sub>2.5</sub> and PM<sub>10</sub> of Lhasa city, the Tibetan  
655 Plateau, *Atmospheric Environment*, 127, 340-346, 2016a.

656 Li, C., Bosch, C., Kang, S., Andersson, A., Chen, P., Zhang, Q., Cong, Z., Chen, B., Qin, D., and  
657 Gustafsson, Ö.: Sources of black carbon to the Himalayan–Tibetan Plateau glaciers, *Nature*  
658 *Communications*, 7, 12574, 2016b.

659 Li, J., Lin, T., Qi, S., Zhang, G., Liu, X., and Li, K.: Evidence of local emission of organochlorine  
660 pesticides in the Tibetan plateau, *Atmospheric Environment*, 42, 7397-7404, 2008.

661 Li, Y., Wang, Y., Li, Y., Li, T., Mao, H., Talbot, R., Nie, X., Wu, C., Zhao, Y., and Hou, C.: Characteristics  
662 and potential sources of atmospheric particulate mercury in Jinan, China, *Science of The Total*  
663 *Environment*, 574, 1424-1431, 2017.

664 Lin, H., Tong, Y., Yin, X., Zhang, Q., Zhang, H., Zhang, H., Chen, L., Kang, S., Zhang, W., and Schauer,  
665 J.: First measurement of atmospheric mercury species in Qomolangma Natural Nature Preserve,  
666 Tibetan Plateau, and evidence of transboundary pollutant invasion, *Atmospheric Chemistry and*  
667 *Physics*, 19, 1373-1391, 2019.

668 Lin, H., Tong, Y., Yu, C., Chen, L., Yin, X., Zhang, Q., Kang, S., Luo, L., Schauer, J., de Foy, B. J. A. C.,  
669 and Physics: First observation of mercury species on an important water vapor channel in the  
670 southeastern Tibetan Plateau, 22, 2651-2668, 2022.

671 Lindberg, S., Bullock, R., Ebinghaus, R., Engstrom, D., Feng, X., Fitzgerald, W., Pirrone, N., Prestbo,  
672 E., and Seigneur, C.: A synthesis of progress and uncertainties in attributing the sources of mercury  
673 in deposition, *AMBIO: a Journal of the Human Environment*, 36, 19-33, 2007.

674 Lindberg, S. a. and Stratton, W.: Atmospheric mercury speciation: concentrations and behavior of  
675 reactive gaseous mercury in ambient air, *Environmental Science & Technology*, 32, 49-57, 1998.

676 Liu, B., Keeler, G. J., Dvonch, J. T., Barres, J. A., Lynam, M. M., Marsik, F. J., and Morgan, J. T. J. A. E.:  
677 Temporal variability of mercury speciation in urban air, 41, 1911-1923, 2007.

678 Liu, N., Qiu, G., Landis, M. S., Feng, X., Fu, X., and Shang, L.: Atmospheric mercury species measured  
679 in Guiyang, Guizhou province, southwest China, *Atmospheric Research*, 100, 93-102, 2011.

680 Liu, S., Nadim, F., Perkins, C., Carley, R. J., Hoag, G. E., Lin, Y., and Chen, L.: Atmospheric mercury  
681 monitoring survey in Beijing, China, *Chemosphere*, 48, 97-107, 2002.

682 Luo, Y., Duan, L., Driscoll, C. T., Xu, G., Shao, M., Taylor, M., Wang, S., and Hao, J. J. J. o. G. R. B.:  
683 Foliage/atmosphere exchange of mercury in a subtropical coniferous forest in south China, 121,  
684 2006-2016, 2016.

685 Lynam, M. M., Dvonch, J. T., Hall, N. L., Morishita, M., and Barres, J. A.: Spatial patterns in wet and  
686 dry deposition of atmospheric mercury and trace elements in central Illinois, USA, *Environmental*  
687 *Science and Pollution Research*, 21, 4032-4043, 2014.

688 Pant, N., Ravindra, R., Srivastava, D., and Thompson, L.: The Himalayan cryosphere: past and  
689 present variability of the 'third pole', Geological Society, London, Special Publications, 462, SP462.  
690 413, 2018.

691 Pokhrel, B., Gong, P., Wang, X., Gao, S., Wang, C., and Yao, T.: Sources and environmental

692 processes of polycyclic aromatic hydrocarbons and mercury along a southern slope of the Central  
693 Himalayas, Nepal, *Environmental Science and Pollution Research*, 23, 13843-13852, 2016.  
694 Qiu, J.: China: the third pole, *Nature News*, 454, 393-396, 2008.  
695 Rhode, D., Madsen, D. B., Brantingham, P. J., and Dargye, T.: Yaks, yak dung, and prehistoric human  
696 habitation of the Tibetan Plateau, *Developments in Quaternary Sciences*, 9, 205-224, 2007.  
697 Rutter, A. P. and Schauer, J. J.: The impact of aerosol composition on the particle to gas partitioning  
698 of reactive mercury, *Environmental science & technology*, 41, 3934-3939, 2007.  
699 Rutter, A. P., Schauer, J. J., Lough, G. C., Snyder, D. C., Kolb, C. J., Von Klooster, S., Rudolf, T.,  
700 Manolopoulos, H., and Olson, M. L.: A comparison of speciated atmospheric mercury at an urban  
701 center and an upwind rural location, *Journal of Environmental Monitoring*, 10, 102-108, 2008.  
702 Seigneur, C., Vijayaraghavan, K., and Lohman, K.: Atmospheric mercury chemistry: Sensitivity of  
703 global model simulations to chemical reactions, *Journal of Geophysical Research: Atmospheres*,  
704 111, 2006.  
705 Selin, N. E.: Global biogeochemical cycling of mercury: a review, *Annual Review of Environment  
706 and Resources*, 34, 43, 2009.  
707 Slemr, F., Angot, H., Dommergue, A., Magand, O., Barret, M., Weigelt, A., Ebinghaus, R., Brunke,  
708 E.-G., Pfaffhuber, K. A., and Edwards, G.: Comparison of mercury concentrations measured at  
709 several sites in the Southern Hemisphere, *Atmospheric Chemistry and Physics*, 15, 3125-3133,  
710 2015.  
711 Song, S., Angot, H., Selin, N. E., Gallée, H., Sprovieri, F., Pirrone, N., Helmig, D., Savarino, J., Magand,  
712 O., and Dommergue, A.: Understanding mercury oxidation and air-snow exchange on the East  
713 Antarctic Plateau: a modeling study, 2018.  
714 Sprovieri, F., Gratz, L., and Pirrone, N.: Development of a ground-based atmospheric monitoring  
715 network for the Global Mercury Observation System (GMOS), *E3S Web of Conferences*,  
716 Sprovieri, F., Pirrone, N., Bencardino, M., D'Amore, F., Carbone, F., Cinnirella, S., Mannarino, V.,  
717 Landis, M., Ebinghaus, R., and Weigelt, A.: Atmospheric mercury concentrations observed at  
718 ground-based monitoring sites globally distributed in the framework of the GMOS network,  
719 *Atmospheric Chemistry and Physics*, 16, 11915-11935, 2016.  
720 Steffen, A., Douglas, T., Amyot, M., Ariya, P., Aspmo, K., Berg, T., Bottenheim, J., Brooks, S., Cobbett,  
721 F., and Dastoor, A.: A synthesis of atmospheric mercury depletion event chemistry in the  
722 atmosphere and snow, *Atmospheric Chemistry and Physics*, 8, 1445-1482, 2008.  
723 Stein, A., Draxler, R. R., Rolph, G. D., Stunder, B. J., Cohen, M., and Ngan, F.: NOAA's HYSPLIT  
724 atmospheric transport and dispersion modeling system, *Bulletin of the American Meteorological  
725 Society*, 96, 2059-2077, 2015.  
726 Stylo, M., Alvarez, J., Dittkrist, J., and Jiao, H.: Global review of mercury monitoring networks, UNEP,  
727 Geneva, 2016.  
728 Swartzendruber, P., Jaffe, D., and Finley, B.: Improved fluorescence peak integration in the Tekran  
729 2537 for applications with sub-optimal sample loadings, *Atmospheric Environment*, 43, 3648-  
730 3651, 2009.  
731 Tibet Bureau of Statistics, T.: *Tibet Statistics Yearbook*, China Statistics Press, Beijing 2020.  
732 Travnikov, O., Angot, H., Artaxo, P., Bencardino, M., Bieser, J., D'Amore, F., Dastoor, A., Simone, F.  
733 D., Diéguez, M. d. C., and Dommergue, A.: Multi-model study of mercury dispersion in the  
734 atmosphere: atmospheric processes and model evaluation, *Atmospheric Chemistry and Physics*,  
735 17, 5271-5295, 2017.

736 UNEP, U. G. M. A.: Sources, Emissions, Releases and Environmental Transport; UNEP Chemicals  
737 Branch: Geneva, Switzerland, 2013, There is no corresponding record for this reference, 2013.

738 Venter, A., Beukes, J., Van Zyl, P., Brunke, E.-G., Labuschagne, C., Slemr, F., Ebinghaus, R., and Kock,  
739 H.: Statistical exploration of gaseous elemental mercury (GEM) measured at Cape Point from 2007  
740 to 2011, *Atmospheric Chemistry and Physics*, 15, 10271-10280, 2015.

741 Wang, C., Wang, X., Gong, P., and Yao, T.: Long-term trends of atmospheric organochlorine  
742 pollutants and polycyclic aromatic hydrocarbons over the southeastern Tibetan Plateau, *Science  
743 of the Total Environment*, 624, 241-249, 2018.

744 Wang, X., Zhang, H., Lin, C. J., Fu, X., Zhang, Y., and Feng, X.: Transboundary transport and  
745 deposition of Hg emission from springtime biomass burning in the Indo-China Peninsula, *Journal  
746 of Geophysical Research: Atmospheres*, 120, 9758-9771, 2015.

747 Xiao, Q., Saikawa, E., Yokelson, R. J., Chen, P., Li, C., and Kang, S.: Indoor air pollution from burning  
748 yak dung as a household fuel in Tibet, *Atmospheric Environment*, 102, 406-412,  
749 10.1016/j.atmosenv.2014.11.060, 2015.

750 Yang, J., Kang, S., Ji, Z., and Chen, D.: Modeling the origin of anthropogenic black carbon and its  
751 climatic effect over the Tibetan Plateau and surrounding regions, *Journal of Geophysical Research:  
752 Atmospheres*, 123, 671-692, 2018.

753 Yang, Y., Chen, H., and Wang, D.: Spatial and temporal distribution of gaseous elemental mercury  
754 in Chongqing, China, *Environmental monitoring and assessment*, 156, 479-489, 2009.

755 Yao, T., Thompson, L. G., Mosbrugger, V., Zhang, F., Ma, Y., Luo, T., Xu, B., Yang, X., Joswiak, D. R.,  
756 and Wang, W.: Third pole environment (TPE), *Environmental Development*, 3, 52-64, 2012.

757 Yin, X., Kang, S., Foy, B. d., Ma, Y., Tong, Y., Zhang, W., Wang, X., Zhang, G., and Zhang, Q.: Multi-  
758 year monitoring of atmospheric total gaseous mercury at a remote high-altitude site (Nam Co,  
759 4730 m asl) in the inland Tibetan Plateau region, *Atmospheric Chemistry and Physics*, 18, 10557 -  
760 10574, 2018.

761 Yin, X., Zhou, W., Kang, S., de Foy, B., Yu, Y., Xie, J., Sun, S., Wu, K., and Zhang, Q.: Latest  
762 observations of total gaseous mercury in a megacity (Lanzhou) in northwest China, *Science of The  
763 Total Environment*, 720, 137494, 2020a.

764 Yin, X., Zhou, W., Kang, S., de Foy, B., Yu, Y., Xie, J., Sun, S., Wu, K., and Zhang, Q. J. S. o. T. T. E.:  
765 Latest observations of total gaseous mercury in a megacity (Lanzhou) in northwest China, 720,  
766 137494, 2020b.

767 Zhang, H., Fu, X., Lin, C., Wang, X., and Feng, X.: Observation and analysis of speciated atmospheric  
768 mercury in Shangri-La, Tibetan Plateau, China, *Atmos. Chem. Phys*, 15, 653-665, 2015a.

769 Zhang, H., Fu, X., Lin, C.-J., Shang, L., Zhang, Y., Feng, X., and Lin, C.: Monsoon-facilitated  
770 characteristics and transport of atmospheric mercury at a high-altitude background site in  
771 southwestern China, *Atmospheric Chemistry & Physics*, 16, 2016.

772 Zhang, L., Wang, S., Wang, L., and Hao, J.: Atmospheric mercury concentration and chemical  
773 speciation at a rural site in Beijing, China: implications of mercury emission sources, *Atmospheric  
774 Chemistry and Physics*, 13, 10505-10516, 2013.

775 Zhang, R., Wang, H., Qian, Y., Rasch, P. J., Easter, R. C., Ma, P.-L., Singh, B., Huang, J., and Fu, Q.:  
776 Quantifying sources, transport, deposition, and radiative forcing of black carbon over the  
777 Himalayas and Tibetan Plateau, *Atmospheric Chemistry and Physics*, 15, 6205-6223, 2015b.

778 Zhou, H., Hopke, P. K., Zhou, C., and Holsen, T. M. J. S. o. t. T. E.: Ambient mercury source  
779 identification at a New York State urban site: Rochester, NY, 650, 1327-1337, 2019.

780 Zhu, J., Wang, T., Talbot, R., Mao, H., Hall, C., Yang, X., Fu, C., Zhuang, B., Li, S., and Han, Y.:  
781 Characteristics of atmospheric total gaseous mercury (TGM) observed in urban Nanjing, China,  
782 Atmospheric Chemistry and Physics, 12, 12103-12118, 2012.  
783 Zhu, J., Xia, X., Che, H., Wang, J., Cong, Z., Zhao, T., Kang, S., Zhang, X., Yu, X., Zhang, Y. J. A. C.,  
784 and Physics: Spatiotemporal variation of aerosol and potential long-range transport impact over  
785 the Tibetan Plateau, China, 19, 14637-14656, 2019.  
786 •